# Sympathetic crystallization of $CaH^+$ produced by a laser-induced reaction

Naoki Kimura,[1] Kunihiro Okada,[1,*] Toshinobu Takayanagi,[1] Michiharu Wada,[2] Shunsuke Ohtani,[3] and Hans A. Schuessler[4]

[1]*Department of Physics, Sophia University, 7-1 Kioicho, Chiyoda, Tokyo 102-8554, Japan*

[2]*Atomic Physics Laboratory, RIKEN, 2-1 Hirosawa, Wako, Saitama 351-0198, Japan*

[3]*Institute for Laser Science (ILS), University of Electro-Communications, 1-5-1 Chofugaoka, Chofu, Tokyo, 182-8585, Japan*

[4]*Department of Physics, Texas A&M University, College Station, Texas 77843, USA*

(Received 7 December 2010; published 30 March 2011)

We investigated sympathetic Coulomb crystallization of $CaH^+$ ions produced by a laser-induced reaction through an excited state according to $^{40}Ca^+(4p\,^2P_{1/2}) + H_2 \rightarrow {}^{40}CaH^+ + H$. $^{40}CaH^+$ ions stored in a linear Paul trap were characterized by their secular-motion excitation spectrum and by the modified fluorescence images of crystallized $Ca^+$ ions. The number of two-species crystallized ions, the secular motion temperature, and the structure were determined by molecular dynamics simulations. Both the observed two-species ion crystals and simulation images demonstrate that the $CaH^+$ ions were sympathetically crystallized with their secular-motion temperature being less than 10 mK. We determined reaction rates from fluorescence images of two-species Coulomb crystals by systematically changing the reaction time. In addition a lower limit for the reaction rate coefficient $k = 8 \times 10^{-10}$ cm$^3$/s was obtained.

DOI: 10.1103/PhysRevA.83.033422 PACS number(s): 37.10.Rs, 37.10.Mn, 34.50.Lf, 52.27.Gr

## I. INTRODUCTION

Cold molecules are attractive research objects for precision spectroscopy of vibrational and rotational transitions and for the study of chemical reactions at very low temperatures. In particular, fundamental physics questions can be addressed by measurements on cold molecules and molecular ions floating practically unperturbed at very low temperature in free space. For instance, the possibility to test the time variation of the proton-electron mass ratio ($m_p/m_e$) using ultracold dimers of alkali-metal atoms, such as $Cs_2$ and $Sr_2$, was proposed [1,2]. Recently, Kajita *et al.* also proposed a new scheme to perform precision spectroscopy of pure vibrational transitions of a single cold molecular ion, $^{40}CaH^+$, using quantum logic spectroscopy [3,4]. With such experiments it may be possible to test a possible time variation of $m_p/m_e$. The attainable uncertainty of such frequency measurements was estimated to be on the order of $10^{-16}$. Moreover calcium hydride is an astrophysically important molecule and has been detected in the Sun and some stars [5]. In this connection ionized $CaH^+$ also plays an important role in the chemical evolution in interstellar clouds [6].

In the field of astrochemistry, the reaction rate coefficients of cold chemical reactions as well as a reaction-network model in interstellar clouds is of interest to understand their chemical evolution. For such purposes the database of the chemical reactions related to astrochemistry have been set up [7]. However, the information in this database is not detailed enough for specific circumstances. Actually, it was pointed out that rate coefficients of ion–polar-molecule reactions are not sufficiently well known to prove the following scenario: a static picture of physical conditions without consideration of interactions with grain surfaces is inappropriate for a complete understanding of the chemistry [8]. In view of the recent rapidly improving astronomical observation technology, such as the Atacama Large Millimeter Array (ALMA), it is important to measure reaction rate coefficients of cold ion–polar-molecule reactions including astrochemically important molecules.

Recently a new method for studying cold ion–polar-molecule reactions was performed for the measurement of the $Ca^+ + CH_3F \rightarrow CaF^+ + CH_3$ reaction [9]. In this experiment, slow polar molecules were produced by a Stark velocity filter and the cold $Ca^+$ target was prepared in a linear Paul trap using laser cooling. This method can be extended to the study of a multitude of cold reactions when combined with sympathetic cooling of molecular ions. In this connection it is important to produce various cold molecular ions in a linear Paul trap as targets for cold chemical reactions.

Here we report experimental results of sympathetic cooling of molecular $CaH^+$ ions in a linear Paul trap and measurements of the production rate of $CaH^+$ by a laser-induced reaction. We successfully produced $CaH^+$ and observed the sympathetic crystallization. The characterization of two-species Coulomb crystals was performed by comparing experimental fluorescence images to calculated crystal images using molecular dynamics simulations [10]. Finally, the reaction rates of the laser-induced reaction were measured under typical experimental conditions and the reaction rate coefficient for room temperature was deduced.

## II. EXPERIMENT

The detailed description of our experimental setup is described in a previous paper [10,11]. Here we present a brief summary of the present improved setup. For laser cooling of the stored $Ca^+$ ions two grating stabilized laser diodes ($\lambda = 397$ and 866 nm) are used and are incident along the trap axis ($z$ axis). Both lasers are locked to a frequency-stabilized helium-neon (He-Ne) laser (Research Electro-Optics, Inc.) through a transfer cavity [12,13]. With this stable laser arrangement an ion crystal can be sustained during more than half day as long as the cryogenic temperature of the trap region is maintained, where the liquid nitrogen baffle was used as an auxiliary cryopump to obtain and sustain the UHV

*Corresponding author: okada-k@sophia.ac.jp

 

condition. The relative frequencies of the lasers are determined by monitoring the cavity signals. A laser-induced fluorescence (LIF) image at 397 nm is observed by a cooled charge coupled device (CCD) camera at a right angle to the trap axis. The camera is mounted on a precision stage outside the vacuum chamber to adjust the imaging position. According to the requirement, the magnification of the lens system is selected to be 3× or 10×.

In addition to the CCD camera we simultaneously observe LIF photons with a photomultiplier tube (PMT) at 45° to the trap axis. Using the PMT a secular motion excitation mass spectrum can be measured by applying the characteristic perturbation rf voltages to one of the trap rods [14,15]. In the measurements, the change of the LIF intensity is measured as a function of the perturbation rf frequency. If the frequency is resonant with a secular motion frequency of sympathetically cooled molecular ions, those ions are heated, and this heating is transferred sympathetically to $^{40}Ca^+$ ions through the Coulomb interaction. In such an optically detected secular scan, the fluorescence intensity of $Ca^+$ ions decreases (or increases) due to the changing Doppler width of the cooling transition. The present two-species Coulomb crystals consisting of $Ca^+$ and $CaH^+$ were analyzed by this sympathetic heating method.

$CaH^+$ is produced by the chemical reaction between the crystallized $Ca^+$ ions and $H_2$ gas as follows:

$$Ca^+(4p\,^2P_{1/2}) + H_2 \rightarrow CaH^+ + H. \quad (1)$$

Similar processes for producing $MgH^+$ and $BeH^+$ have been demonstrated [16,17]. For producing $CaH^+$, $H_2$ gas of nominal pressure on the order of $10^{-6}$ Pa at room temperature was leaked into the vacuum chamber, where we measured the partial pressure at an extra port of the vacuum chamber. Since the reaction is endothermic by about 2.27 eV for the ground state of $Ca^+$ [18], the reaction never proceeds without laser excitations to the $4p^2P_{1/2}$ state, and therefore the cooling lasers ($\lambda = 397$ and 866 nm) must be incident on the ion crystal for the production of $^{40}CaH^+$ ions. The energy difference between the reaction enthalpy (2.27 eV) and the excitation energy (3.1 eV at $\lambda = 397$ nm) is 0.83 eV. Since the pseudopotential of the linear trap exceeds 2 eV, a part of generated $CaH^+$ ions are trapped and are quickly cooled by the ion-ion Coulomb interaction with the laser-cooled $Ca^+$ ions.

## III. CHARACTERIZATION OF ION COULOMB CRYSTALS

We determined the number of ions in an ion Coulomb crystal by applying the following two methods. On one hand, for large $Ca^+$ Coulomb crystals with an ion number of more than $N > 2000$ ions, the ion number density $n_q$ at 0 K in a linear Paul trap was calculated [10]. The number of $Ca^+$ ions is determined by the product of $n_q$ and the volume of a Coulomb crystal which can be determined from the size of a fluorescence image. In the case of large two-species crystals including $Ca^+$ and $CaH^+$, it was difficult to determine the absolute number of each ion species under the present conditions due to the existence of the weak asymmetric fields in the radial direction. However, it is sufficient to determine the relative number of $Ca^+$ ions for the reaction rate measurement of reaction (1). The detailed procedure will be explained later.

On the other hand, the number of ions for a small Coulomb crystal is determined by molecular dynamics (MD) simulations. The details of the simulation are described in our previous papers [10,19]. Here we briefly summarize the method. Newton's equations of motion for all trapped ions are numerically solved under the pseudopotential approximation. Instead of the radiation pressure force for including the laser cooling effect and collisions with residual background gases for producing the heating effect, we introduce cold elastic collisions between trapped ions and virtual very light atoms to produce the observed fluorescence images, where we assume that ion Coulomb crystals are in the thermal equilibrium as long as the observation period by a CCD camera is long enough [10]. For producing a simulation image we divide the image area which corresponds to the size of the CCD image sensor into many small cells. At each integration step we increment a cell counter by one if an ion exists in this cell [20]. The CCD images of the Coulomb crystals are depicted by a density plot of the cells.

In the MD simulation sympathetic cooling of $CaH^+$ ions is achieved by only the Coulomb interaction with cooled $Ca^+$ ions. In order to characterize the two-species Coulomb crystals, we reproduce a deformed fluorescence image by a simulation image, which is obtained by adjusting the secular motion temperature and the number of each ion species in the crystal to yield the proper observed image.

## IV. RESULTS AND DISCUSSION

### A. Mass spectrum

In order to confirm the mass of the product ions, we measured a mass spectrum by secular motion excitation after the $CaH^+$ production process according to reaction (1). Figure 1 shows a mass spectrum of a large two-species Coulomb crystal with about 7500 ions together with the corresponding CCD images after the reaction time of $3.2 \times 10^2$ s. Since the magnification of the observation optics is 3×, the detailed structure of the crystal is not resolved. The optical detected secular excitation spectrum was used to identify the

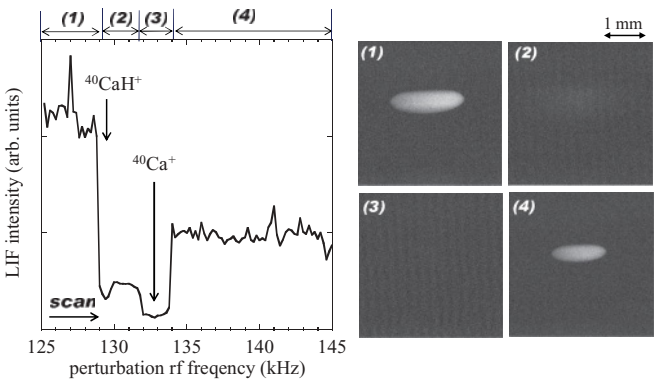


FIG. 1. A secular-motion-excitation mass spectrum of a two-species Coulomb crystal and the snapshots of the fluorescence images corresponding to states (1)–(4) in the mass spectrum. The exposure time of the CCD camera was set to 1 s. The reaction time for producing $CaH^+$ ions was $3.2 \times 10^2$ s. We applied a strong perturbation voltage of 35 mV for secular-motion excitation.

two simultaneously stored ion species [14,15]. In Fig. 1, the rf frequency was swept from 125 to 145 kHz to excite the $Ca^+$ and $CaH^+$ motional frequencies. The signal at about 129 kHz is due to the sympathetic heating from the $CaH^+$ ions. The signal at about 133 kHz is caused by directly heating the $Ca^+$ ions. After the two resonances, the fluorescence intensity recovered showing that the $Ca^+$ ions recrystallized. However the intensity value is somewhat lower than before the secular scan, since the number of $Ca^+$ ions decreased by the strong perturbations. The result of this experiment demonstrates that the product ions are $CaH^+$ ions.

### B. Observation of two-species Coulomb crystals

Figure 2 shows a typical fluorescence image (a) and the corresponding simulation image (b). As opposed to a pure ion crystal of $Ca^+$ which forms a cylindrically symmetric shape along the trap axis [10], the crystal structure of Fig. 2(a) is deformed by the existence of molecular $CaH^+$ ions produced by the laser-induced reaction. $CaH^+$ ions were pushed to the upper side of the image due to the existence of the asymmetric dc voltages by the patch effect of electric charges on the electrodes. In order to take this effect into account in the MD simulation, weak uniform electric fields are added along the $x$ and $y$ directions. The proper correction field strength can be determined by fitting a simulation image to Fig. 2(a). As a result, Fig. 2(b) suggests that the $CaH^+$ ions were sympathetically crystallized and accumulate on the upper side of the ion crystal. The numbers of $Ca^+$ and $CaH^+$ ions are determined to be $N(Ca^+) = 134$ and $N(CaH^+) = 40$, respectively. In this example, the accuracy is better than $\pm 6$ ions.

In the case of a smaller number of ions, the position of each $CaH^+$ ion is precisely determined by the MD simulation. For instance, Fig. 3 shows small two-species Coulomb crystals as well as the corresponding simulation results. In the case of Fig. 3(a), the fluorescence image forms an asymmetric structure relative to the trap axis. The MD simulation shows that seven $CaH^+$ ions are sympathetically crystallized on the upper side of the $Ca^+$ crystal. Figure 3(b) depicts the bent

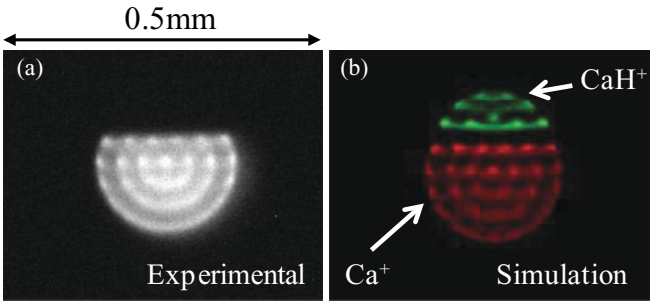


FIG. 2. (Color online) (a) A two-species ion Coulomb crystal consisting of $Ca^+$ and $CaH^+$. The upper side of the image is occupied by $CaH^+$ ions. The rf frequency and the amplitude are $f_{rf} = 5.49$ MHz and $V_{ac} = 171.5$ V, respectively. The static voltage applied to the end electrodes is $V_z = 7.1$ V. (b) A simulation image reproducing the image (a). The numbers of $Ca^+$ and $CaH^+$ are determined to be $N(Ca^+) = 134$ and $N(CaH^+) = 40$, respectively. The correction static fields of $E_x = 40$ mV/mm and $E_y = -40$ mV/mm were added to reproduce the asymmetric image (a). The secular-motion temperature of both ion species is computed to be about 7 mK.

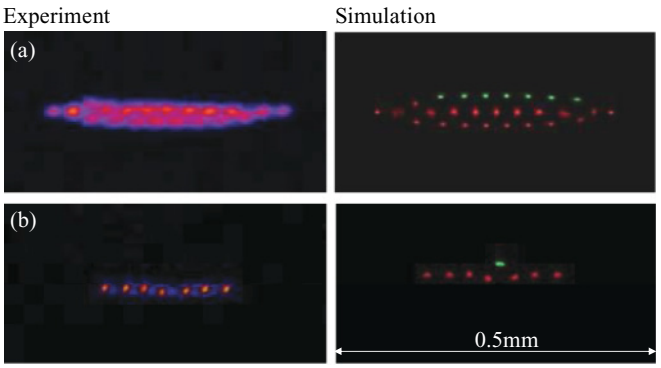


FIG. 3. (Color online) Observed fluorescence images (left) of two-species Coulomb crystals with a small number of ions and the corresponding simulation results (right). The scale of all figures is the same. From the results of the MD simulation, the ion numbers and the upper limit of the secular motion temperature are determined: (a) $N(Ca^+) = 28$, $N(CaH^+) = 7$, $T_{sec} \leqslant 5$ mK; (b) $N(Ca^+) = 7$, $N(CaH^+) = 1$, $T_{sec} \leqslant 8$ mK.

structure of a string crystal due to the existence of a single $CaH^+$ ion. The upper limit of the average secular energy of the single $CaH^+$ is computed to be 8 mK from the simulation result.

### C. Reaction rate measurement

We measured the reaction rate of $^{40}Ca^+(4p\,^2P_{1/2}) + H_2 \rightarrow {}^{40}CaH^+ + H$ under the present experimental conditions and estimated the lower limit of the reaction rate coefficient as described in the following.

Figure 4 shows snapshots of a large $Ca^+$ Coulomb crystal after different reaction times. The initial number of $Ca^+$ before reaction (1) was $(7.3 \pm 0.2) \times 10^3$ ions. The dark area in the upper side of the fluorescence image gradually extended as the reaction time increased. This is caused by the increase of $CaH^+$ ions. As we already mentioned, the weak asymmetric static fields pushed heavier $CaH^+$ ions to the upper side, because the pseudopotential of $CaH^+$ is a little shallower than that of $Ca^+$.

In order to obtain the reaction rate, we determine the relative number of $Ca^+$ ions at each reaction time. In doing this we assumed that the ion number density for $Ca^+$ is not modified by the small number of $CaH^+$ ions because the mass number of $CaH^+$ is very close to that of $Ca^+$. With this reasoning we estimated relative ion numbers which are more relevant than the absolute numbers of $Ca^+$ and $CaH^+$ according to the following procedure.

First, we determined the major and the minor axes of the assumed prolate shape of the fluorescence image, which is indicated as the oval dashed line in Fig. 4. Then the prolate ellipsoidal volume without the dark area was numerically calculated. The relative number of residual $Ca^+$ ions is proportional to the bright volume under conditions of constant ion-number density.

Figure 5(a) describes the decay of the relative number of $Ca^+$ ions in Fig. 4 due to the laser-induced reaction (1). The slope of the decay curve increases after a reaction time of 400 s since the loss rate of the $Ca^+$ becomes larger due to the increasing space-charge of the $CaH^+$ ions. Under these

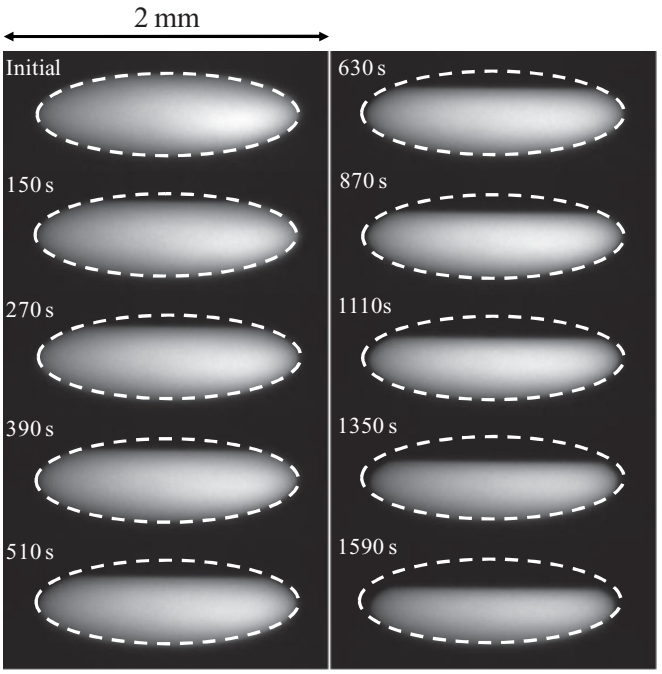


FIG. 4. Systematic observation of fluorescence images of two-species ion Coulomb crystals during reaction (1). In the initial condition a prolate $Ca^+$ Coulomb crystal was produced. As the reaction time increased the dark area in the upper side of the crystal extended. The nominal $H_2$ pressure was $4.8 \times 10^{-6}$ Pa during the measurement. Observation optics with a magnification of 3× was used.

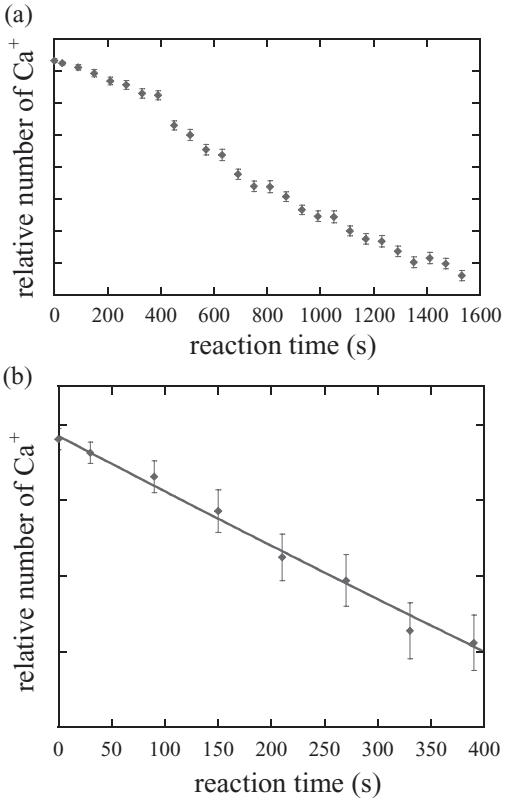


FIG. 5. (a) The decay of the relative number of $Ca^+$ ions in the large ion crystal of Fig. 4 due to the laser-induced reaction (1). The relative number of $Ca^+$ ions is obtained by estimating the volume of the fluorescence images in Fig. 4. It is clearly seen that the slope of the decay curve changes at about 400 s. (b) A least-square fit analysis of the initial slope yields the reaction rate. The error is estimated by the uncertainties of the volume determination of the $Ca^+$ crystals. The data at reaction times less than 400 s in panel (a) was used. A reaction rate of $(1.9 \pm 0.8) \times 10^{-4}$ $s^{-1}$ was obtained.

conditions stronger rf heating and a decrease of the laser cooling rate occur. Therefore only data for reaction times less than 400 s in Fig. 5 were used to obtain the reaction rate, as is shown in Fig. 5(b). Using least-square fitting of the exponential curve $N(Ca^+) = N_0(Ca^+)e^{-\gamma t}$ in several sets of data the reaction rate is determined as $\gamma = (1.9 \pm 0.8) \times 10^{-4} s^{-1}$. The reaction rate coefficient $k$ is related to $\gamma = k\rho_e n_{H_2}$, where $n_{H_2}$ and $\rho_e$ are the number density of $H_2$ gas and the excited state population of the $^2P_{1/2}$ state, respectively. In general $k$ describes the reaction constant better than $\gamma$ and there is not large dependence on the temperatures for ion-molecule reactions. It is pointed out that the change of the slope in decay curves may change for different sizes of ion crystals because the loss rate of $Ca^+$ ions depends on the competition between the rf heating effect and the laser cooling effect.

For the case of small Coulomb crystals ($N_{ion} \leqslant 100$), a MD simulation was applied to determine the numbers of $Ca^+$ and $CaH^+$ in mixed ion crystals. Figure 6 shows observed fluorescence images of two-species Coulomb crystals after starting the reaction (1) at the nominal $H_2$ pressure of $4.8 \times 10^{-6}$ Pa. In the present measurement, the intentionally loaded $H_2$ gas was evacuated at every image observation to cool the $Ca^+$ ions before the next reaction process, since the ion crystal was slightly heated by collisions with $H_2$ and the inside structure of the crystal became obscure.

The numbers of $Ca^+$ and $CaH^+$ ions were determined by fitting simulation images to the fluorescence image [Fig. 6(b)]. As a result, we obtain the number of each ion species as a function of the reaction time (Fig. 7). From the decay curve of $Ca^+$, the reaction rate of $\gamma = (6.1 \pm 0.2) \times 10^{-4}$ $s^{-1}$ is determined. Since we took typically 25 s to evacuate and load the $H_2$ gas, the uncertainty of the reaction time (±25 s) was considered to determine the reaction rate. It is noted that for small ion crystals the reaction rate is larger than for large ion crystals. This is due to a higher excitation rate in the *S*-*P* transition for smaller crystals.

The uv laser-detuning dependence on the reaction rates was also measured for some large and small two-species crystals under the same conditions as the above measurements. A compilation of the measurements is shown in Fig. 8. Generally the reaction rate increases as the uv laser detuning ($\Delta\nu_{uv}$) decreases until reaching the optimum detuning of half of the natural linewidth (HWHM 11 MHz), because the population in the $^2P_{1/2}$ state increases by decreasing the ion temperature. In fact, at the same laser-detuning (40 MHz) the reaction rate of the small Coulomb crystal [Fig. 8(c)] was higher than that of the large crystal [Fig. 8(d)]. This result implies that a smaller ion crystal is cooled to a lower temperature and the $^2P_{1/2}$ population is larger at the same $\Delta\nu_{uv}$.

Finally we deduce the reaction rate coefficient $k$ of $^{40}Ca^+(4p\,^2P_{1/2}) + H_2 \rightarrow {}^{40}CaH^+ + H$. Using the nominal $H_2$ pressure of $4.8 \times 10^{-6}$ Pa in the vacuum chamber and

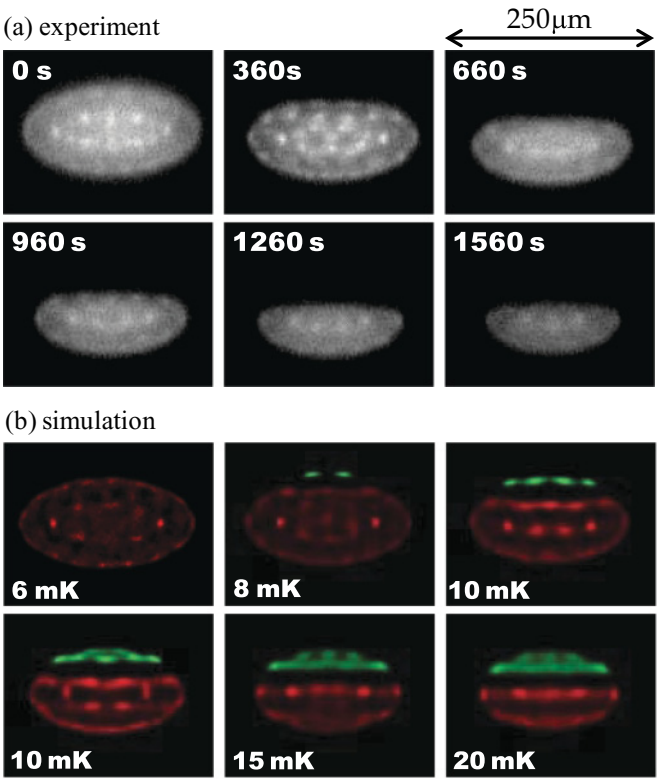


FIG. 6. (Color online) Systematic observation of fluorescence images of two-species small Coulomb crystals. The images were observed using the lens system with 10× magnification. The corresponding simulation images are also shown in the lower images (b). The reaction time and the assumed secular-motion temperatures in the MD simulations are indicated in the images. During the measurements the nominal pressure of the $H_2$ gas was $4.8 \times 10^{-6}$ Pa. The rf frequency and the amplitude are $f_{\rm rf} = 5.532$ MHz and $V_{\rm ac} = 204.5$ V, respectively. The static voltage applied to the end electrodes is $V_z = 5.3$ V.

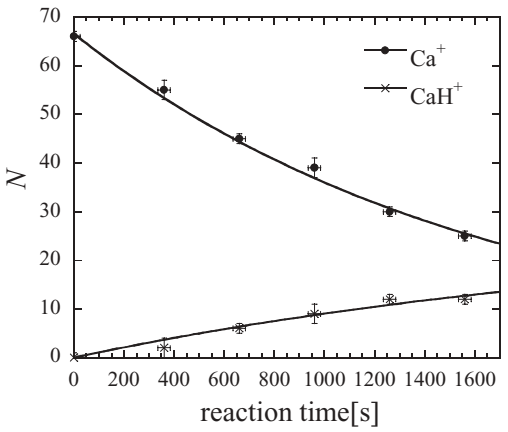


FIG. 7. A plot of the ion numbers of $Ca^+$ and $CaH^+$ contained in the Coulomb crystals as a function of the reaction time. Each point was determined by fitting simulation images to the observed images in Fig. 6. The error of the number of ions is caused by the uncertainty of the fitting results. The uncertainty of the reaction time (typically ±25 s) is the time taken for loading and evacuating the $H_2$ gas. The solid line for $Ca^+$ is the best-fitting exponential curve to sets of the data while the line for $CaH^+$ is just to guide the eye. The reaction rate of $(6.1 \pm 0.2) \times 10^{-4}$ $s^{-1}$ was obtained by the $Ca^+$ decay rate.

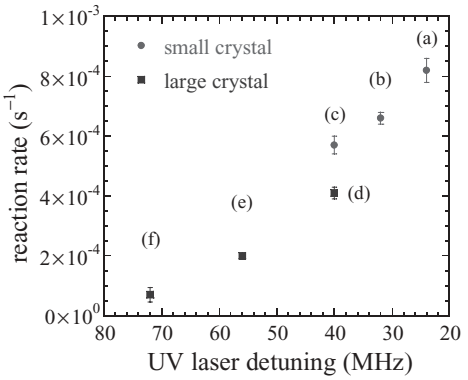


FIG. 8. A plot of the reaction rates as a function of the 397-nm laser detuning. The initial numbers of $Ca^+$ ions were determined by the same method described in the text: (a) $74 \pm 2$, (b) $66 \pm 2$, (c) $94 \pm 2$, (d) $(8.1 \pm 0.2) \times 10^3$, (e) $(7.3 \pm 0.2) \times 10^3$, and (f) $(5.8 \pm 0.1) \times 10^3$. The nominal pressure of $H_2$ ($4.8 \times 10^{-6}$ Pa) is the same for all measurements. The error bars originate from the fitting error of the exponential curve. The error of (e) is $\pm 1 \times 10^{-5}$, which is within the point size.

the data of the maximum reaction rate in Fig. 8, the deduced reaction rate coefficient is $(7.0 \pm 0.3)/\rho_e \times 10^{-13}$ $cm^3/s$. The $^2P_{1/2}$ population $\rho_e$ under the present experimental conditions was evaluated to be about 0.09% with the optical Bloch equation. The value gives the reaction rate coefficient of $8 \times 10^{-10}$ $cm^3/s$, which is on the same order of the Langevin rate, $k_L = 1.5 \times 10^{-9}$ $cm^3/s$. The secular temperatures of small ion crystals during the reactions are deduced to be a few tens of millikelvin from the CCD images. In the case of the large crystal in Fig. 4, it is estimated to be lower than 1 K from the half width of the LIF spectrum obtained while loading $H_2$ gas at room temperature. It should be noted that the present reaction rate coefficient is the lower limit, because the actual pressure of $H_2$ should be slightly lower than the nominal pressure, which was measured on the place next to the cryogenic trap region.

## V. SUMMARY

In summary we have demonstrated the sympathetic crystallization of $CaH^+$ ions when they are simultaneously stored and cooled by $Ca^+$ ions. The present production method of $CaH^+$ by a laser-induced reaction will be useful to perform precision spectroscopy of the vibrational transitions in $CaH^+$ by quantum logic spectroscopy [3].

The fluorescence images of the two-species Coulomb crystals consisting of $Ca^+$ and $CaH^+$ were successfully observed and were characterized by MD simulations. By comparing to the simulation images, the structure and the secular-motion temperatures of observed two-species crystals were determined. Additionally we found that the minimum secular-motion temperature of sympathetically cooled $CaH^+$ ions is as low as 10 mK. Finally we measured the reaction rate of $^{40}Ca^+(4p\,^2P_{1/2}) + H_2 \rightarrow {}^{40}CaH^+ + H$ using the observed images, and a lower limit of the reaction rate coefficient was obtained.

In principle many other molecular ions ($N_2^+$, $NH_3^+$, $NH_4^+$, $H_3O^+$, etc.) can also be sympathetically cooled using the present setup by applying some ionization methods, such as photoionization or electron bombardment. Therefore a variety of cold molecular ions can be used as a cold target for studying molecular-ion–polar-molecule collisions using a Stark velocity filter [21] and other methods such as a rapidly rotating nozzle producing slow molecular pulsed beams [22–24]. We plan to perform measurements of cold ion–polar-molecule reactions using these sympathetically cooled molecular ions. For this purpose we have recently developed a Stark velocity filter and succeeded in producing cold $ND_3$, $NH_3$, and $CH_2O$ molecules with a peak velocity of about 30 m/s [25].

## ACKNOWLEDGMENTS

The authors thank Dr. Kensuke Matsubara, Dr. Minori Abe, and Dr. Masatoshi Kajita for useful discussions. This work is financially supported in part by a Grant-in-Aid for Young Scientists (A) from the Ministry of Education, Culture, Sports, Science and Technology (MEXT) and by the Robert A. Welch Foundation under Grant A1546.

[1] D. DeMille, S. Sainis, J. Sage, T. Bergeman, S. Kotochigova, and E. Tiesinga, Phys. Rev. Lett. **100**, 043202 (2008).
[2] T. Zelevinsky, S. Kotochigova, and J. Ye, Phys. Rev. Lett. **100**, 043201 (2008).
[3] M. Kajita and Y. Moriwaki, J. Phys. B **42**, 154022 (2009).
[4] P. O. Schmidt, T. Rosenband, C. Langer, W. M. Itano, J. C. Bergquist, and D. J. Wineland, Science **309**, 749 (2005).
[5] S. Lepine, R. Michael Rich, and M. M. Shara, Astrophys. J. **591**, L49 (2003).
[6] D. Petiprez, B. Lemoine, C. Demuynck, J. L. Destombes, and B. Macke, J. Chem. Phys. **91**, 4462 (1989).
[7] J. Woodall, M. Agundez, A. J. Markwick-Kemper, and T. J. Millar, Astron. Astrophys. **466**, 1197 (2007).
[8] V. Wakelam, E. Herbst, and F. Selsis, Astron. Astrophys. **444**, 883 (2005); **451**, 551 (2006).
[9] S. Willitsch, M. T. Bell, A. D. Gingell, S. R. Procter, and T. P. Softley, Phys. Rev. Lett. **100**, 043203 (2008).
[10] K. Okada, M. Wada, T. Takayanagi, S. Ohtani, and H. A. Schuessler, Phys. Rev. A **81**, 013420 (2010).
[11] K. Okada, T. Takayanagi, M. Wada, S. Ohtani, and H. A. Schuessler, Phys. Rev. A **80**, 043405 (2009).
[12] W. Z. Zhao, J. E. Simsarian, L. A. Orozco, and G. D. Sprousea, Rev. Sci. Instrum. **69**, 3737 (1998).
[13] K. Matsubara and S. Uetake, H. Ito, Y. Li, K. Hayasaka, and M. Hosokawa, Jpn. J. Appl. Phys. **44**, 229 (2005).
[14] X. Zhao, V. L. Ryjkov, and H. A. Schuessler, Phys. Rev. A **66**, 063414 (2002).
[15] K. Okada, M. Wada, T. Nakamura, T. Takayanagi, I. Katayama, and S. Ohtani, Jpn. J. Appl. Phys. **45**, 951 (2006).
[16] K. Mølhave and M. Drewsen, Phy. Rev. A **62**, 011401(R) (2000).
[17] B. Roth, P. Blythe, H. Wenz, H. Daerr, and S. Schiller, Phys. Rev. A **73**, 042712 (2006).
[18] The reaction enthalpy of the $^{40}Ca^+ + H_2 \rightarrow CaH^+ + H$ reaction at 0 K was estimated using the Gaussian 03 program package (M. J. Frisch *et al.*, Gaussian 03 Revision B.01, Gaussian, Inc. Pittsburgh, PA, 2003). The geometry optimization of molecular ions and calculations of zero-point energies were performed by B3LYP/6-31G(d). The ground state energies were calculated using B3LYP/6-311+($3df$, $3pd$) with optimized geometries.
[19] K. Okada, K. Yasuda, T. Takayanagi, M. Wada, H. A. Schuessler, and S. Ohtani, Phys. Rev. A **75**, 033409 (2007).
[20] C. B. Zhang, D. Offenberg, B. Roth, M. A. Wilson, and S. Schiller, Phys. Rev. A **76**, 012719 (2007).
[21] S. A. Rangwala, T. Junglen, T. Rieger, P. W. H. Pinkse, and G. Rempe, Phys. Rev. A **67**, 043406 (2003).
[22] M. Gupta and D. Herschbach, J. Phys. Chem. A **103**, 10670 (1999).
[23] M. Gupta and D. Herschbach, J. Phys. Chem. A **105**, 101626 (2001).
[24] M. Strebel, F. Stienkemeier, and M. Mudrich, Phys. Rev. A **81**, 033409 (2010).
[25] K. Okada *et al.* (unpublished).